DENTAL MATERIALS 35 (2019) 74–86

Available online at www.sciencedirect.com

ScienceDirect

journal homepage: www.intl.elsevierhealth.com/journals/dema

Assessing the osteogenic potential of zirconia and titanium surfaces with an advanced *in vitro* model

Markus Rottmar[a,1], *Eike Müller*[a,1], *Stefanie Guimond-Lischer*[a], *Marc Stephan*[b], *Simon Berner*[b], *Katharina Maniura-Weber*[a,*]

[a] *Empa, Swiss Federal Laboratories for Materials Science and Technology, Biointerfaces, St. Gallen, Switzerland*
[b] *Institut Straumann AG, Basel, Switzerland*

ARTICLE INFO

Article history:
Received 4 May 2018
Received in revised form
12 September 2018
Accepted 12 October 2018

Keywords:
Zirconia
Implant
Blood coagulation
Primary human bone cells
Osseointegration

ABSTRACT

Objectives. In recent years, zirconia dental implants have gained increased attention especially for patients with thin gingival biotypes or patients seeking metal-free restoration. While physical and chemical material surface properties govern the blood-material interaction and subsequent osseointegration processes, the organizational principles underlying the interplay of biochemical and biophysical cues are still not well understood. Therefore, this study investigated how the interaction of a microstructured zirconia surface with blood influences its osseointegration potential compared to microstructured titanium with or without additional nanostructures.

Methods. Microstructured zirconia and micro- (and nano)structured titanium surfaces were fabricated *via* sandblasting followed by acid etching and their topographical as well as physico-chemical features were thoroughly characterized. Following, an advanced *in vitro* approach mimicking the initial blood interaction of material surfaces upon implantation was applied. Fibrinogen adsorption, human blood coagulation as well as their influence on cell fate decisions of primary human bone and progenitor cells (HBC) were studied.

Results. Obtained surface micro- and nanostructures on titanium surfaces were sharp with rugged peaks whereas zirconia surfaces were less rough with structures being shallower, more round and granular. Compared to titanium surfaces, the zirconia surface showed increased fibrinogen adsorption, higher levels of total accessible fibrinogen γ-chain moieties yielding in increased platelet adhesion and activation and consequently thrombogenicity. Mineralization of HBC on microstructured surfaces was significantly higher on zirconia than on titanium, but was significantly lower compared to titanium surfaces with nanostructures.

Significance. This study provides insights into blood-material interaction and subsequent cellular events that are important for implant surface development.

* *Corresponding author at*: Empa, Swiss Federal Laboratories for Materials Science and Technology, Lerchenfeldstrasse 5, 9014 St. Gallen, Switzerland.
E-mail address: katharina.maniura@empa.ch (K. Maniura-Weber).
[1] Equal contribution.
https://doi.org/10.1016/j.dental.2018.10.008

1. Introduction

Dental implants are the gold standard of dental replacement strategies and to date, a multitude of implant materials and surface modifications have been developed and are routinely applied in clinics. Especially titanium and titanium alloys have been the materials of choice for dental implant systems due to their exceptional mechanical and chemical properties as well as the biological response to those implants [1]. Various *in vitro* and *in vivo* studies successfully showed that the implant surface properties including topography, chemical composition, and hydrophilicity regulate the cellular fate decisions of osteoprogenitors and their progeny, ultimately determining the osseointegration potential and clinical success of an implant [2]. Microstructuring of titanium surfaces *via* sandblasting and acid etching has been shown to induce osteogenic differentiation *in vitro* [3,4], and also to result in a better osseointegration of the material *in vivo* [5,6]. Interestingly, modification of the microstructured surfaces with additional spontaneously formed nanostructures *via* storage of the freshly prepared surfaces in NaCl solution further increases the osseointegration potential of the materials [6,7]. Not only topographical features, but also surface hydrophilicity was demonstrated to trigger the osteogenic differentiation [6,7]. Combining these surface properties to create super-hydrophilic micro- and nanostructured titanium surfaces results in fastest osseointegration of the material, thus presenting the current gold standard for dental implants [6,8]. The relevance of micro- and/or nanostructured dental implants was ultimately shown by the large number of clinical studies that demonstrate enhanced osseointegration and an overall reduction in healing time [9–11].

Even though titanium based implants have become the standard in clinics, unfavorable outcomes can occur especially in patients having a thin gingival biotype. There, in case of buccal bone loss, the grey color of titanium can appear through the gingiva around the region of an osseointegrated implant [12–15]. Furthermore, few cases of potential titanium intolerance in patients have been described, which would require an alternative material for implant-supported prosthetic rehabilitation [16,17]. In the recent two decades, ceramic implants especially those made of yttria-stabilized tetragonal zirconia polycrystalline (Y-TZP) material have been developed. The tooth-like color of the material, the excellent mechanical properties and demonstrated biocompatibility makes zirconia a promising alternative to titanium implants [18,19]. Preclinical studies show the importance of surface roughness for ceramic implants as it is the case for titanium-based implants [20,21]. Importantly, preclinical and early clinical studies show bone-to-implant contact and removal torque being similar for microstructured ceramic and titanium implants after complete integration into the bone, thus suggesting that both materials offer similar long-term performance [22–25]. Furthermore, on the long-term zirconia implants are suggested to perform similarly to state-of-the-art hydrophilic titanium implants with micro and nanostructures, too [24]. However, the early osseointegration potential (≤4 weeks) of zirconia surfaces in comparision to micro- and nanostructured, hydrophilic titanium implants still remains unclear.

As mentioned before, surface micro- and nanotopography, as well as hydrophilicity have been successfully identified to enhance osseointegration potential of titanium implants. However, surface roughening of zirconia has been technically challenging due to the high hardness of the material and to date, only limited information is available on the influence of zirconia surface design on bone cell fate decisions. Few reports have shown that increasing the surface roughness of zirconia implants has a positive effect on osseointegration, which is similar to what has been observed for titanium surfaces [20,23,26]. Also, rendering hydrophobic zirconia discs hydrophilic *via* UV light treatment was shown to increase attachment, spreading, proliferation, and bone protein expression of rat bone marrow-derived osteoblasts [27]. Furthermore, Caravaca et al. could demonstrate that oxygen plasma treatment followed by silanization could increase the hydrophilicty of zirconia surfaces and improve cell attachment as well as proliferation of osteoblast-like cells (MG-63) [28].

In vitro studies on osseointegration mostly focus on the cellular response toward the bare implant material, which however fails to recapitulate the *in vivo* situation during surgery in which the material is exposed to blood before coming in contact with cells. Immediately upon implantation, proteins of the blood (*e.g.* albumin, immunoglobulins, or fibrinogen) are adsorbed in material dependent concentrations and composition on the implant surfaces [29]. This is followed by a multitude of biological processes including blood coagulation, which is responsible for thrombus formation on top of the material, as well as the immune response [30,31]. The formed thrombus, a mixture of fibrin, blood cells and a mixture of cytokines, on the implant surface provides the first, temporary matrix at the site of injury and has a pivotal role in inflammation, tissue regeneration and integration of the implant [32]. Previous studies demonstrated not only the important role of the implant materials on protein adsorption and thrombus formation [33,34], but also the impact of the blood clot on differentiation of primary human bone and progenitor cells (HBC) [7]. Notably, applying an *in vitro* approach including a blood incubation step prior to HBC culture Kopf et al. obtained an osseointegration potential for the titanium surfaces SLA and SLActive, that correlates very well to the observed osseointegration of the surfaces in an *in vivo* study [6,7]. Therefore, this *in vitro* setup could provide the means to obtain predictive data when evaluating the osseointegration potential of novel implant materials and material surfaces prior *in vivo* studies. The aim of the present study was to investigate how the interaction of a microstructured zirconia surface (ZLA) with blood influences its osseointegration potential compared to microstructured titanium with (SLActive), or without additional nanostructures (SLA). For this, the previously established *in vitro* approach, including the incubation of material surfaces with human whole blood prior cell culture [7] (Fig. 2A), was applied to study fibrinogen adsorption, blood coagulation as well as cell fate decisions of HBC on blood pre-incubated surfaces. Given the expected predictive value of the herein presented results, this study provides important insights how physico-chemical properties govern the blood-material interaction and subsequent cellular events

that are highly relevant for the development of newly designed zirconia surfaces prior to *in vivo* studies.

2. Materials and methods

2.1. Materials and surface modifications

Samples and surface modifications were prepared by Straumann (Institut Straumann AG). The titanium disc samples were 5 mm in diameter and were prepared from a c.p. titanium sheet grade 2. The ceramic disc samples were 5 mm in diameter and they were made from yttria-stabilized tetragonal zirconia polycrystalline material (3Y-TZP), which is identical to the material of Straumann PURE ceramic implants. The surfaces SLA, SLActive, and ZLA correspond to the SLA®, SLActive®, and ZLA™ implant surfaces and were created according to proprietary processes by Straumann. In brief, the titanium substrates were sandblasted with corundum (particle size 250–500 μm) followed by acid-etching in a boiling mixture of HCl and H_2SO_4. The SLA discs were then cleaned in HNO_3 and rinsed in deionised water. Finally, the SLA surfaces were air dried, wrapped in aluminum foil and packed in peel bags. After acid etching, the further treatment of the SLActive surfaces took place under nitrogen to prevent exposure to air and the samples were finally rinsed in 0.9% NaCl and stored in 0.9% NaCl solution at about pH 5. SLActive surfaces were only used after the spontaneous formation of nanostructures had occurred [35]. Titanium discs were γ-sterilized (25–42 kGy). To produce ZLA surfaces, the zirconia samples were blasted with corundum, then acid-etched in HF, followed by rinsing in deionised water. Finally, the discs were air dried, packed in peel bags and sterilized employing H_2O_2 plasma sterilization.

2.2. Contact angle measurement

The wettability of all sample surfaces was evaluated by contact-angle measurements using a sessile-drop test with ultrapure water (EasyDrop DSA20E, Krüss GmbH) and a droplet size of 0.3 μL. The SLActive samples stored in saline solution were blown dry in a stream of argon prior to the contact angle measurements. The samples stored dry were measured as received. For each type of material, three samples were measured. Contact angles of SLA were determined by fitting a general conic-section equation to the contour of the droplet placed on the surface (tangent method), whereas smaller contact angles of ZLA and SLActive were fitted with a circular function.

2.3. Surface roughness

The surface roughness was analyzed with a confocal microscope (μsurf explorer, NanoFocus AG) equipped with a 20× lens to obtain 3D images with a measurement area of $798 \times 798\ \mu m^2$ and a lateral resolution of 1.56 μm. Three samples per material type were examined at three random positions each. Roughness parameters were calculated using the software μsoft Analysis XT (NanoFocus AG) by applying a Gaussian filter with a cut-off wavelength of $50 \times 50\ \mu m^2$. Five different parameters were selected to characterize the surface topography: S_a (average height deviation from the mean plane), S_z (maximum height), S_{sk} (skewness of the height distribution), S_{dr} (developed surface area), and S_{pd} (density of peaks).

2.4. X-ray photoelectron spectroscopy (XPS)

The chemical composition of the surface (outermost 5–10 nm) was investigated by XPS. The measurements were performed by SuSoS AG, Dübendorf, Switzerland. Spectra were acquired on a PhI5000 VersaProbe spectrometer (ULVAC-PHI, INC.) equipped with a focused scanning monochromatic Al-Kα source (1486.6 eV). The photoelectrons were detected at an angle of 45° to the surface normal by means of a hemispherical analyzer with a multi-channel detection system with 16 channels. Three samples were analyzed for each type of surface modification. Each sample was analyzed on one spot with a spot size of 200 μm scanning an area of $200 \times 1000\ \mu m$ in case of the titanium samples and a spot size of 200 μm in case of the zirconia samples. A survey scan and detailed spectra of the elements observed in the survey were acquired. The SLActive samples stored in saline solution were rinsed with ultrapure water and blown dry in a stream of nitrogen prior to the measurements. The samples stored dry were measured as received without any pretreatment.

2.5. Scanning electron microcopy (SEM)

The surface morphology of the SLA, SLActive, and ZLA samples was investigated by Scanning Electron Microscopy (SEM). Measurements were performed on three different discs for each type of surface modification. Analysis was performed with a Zeiss Supra 55 SEM (Carl Zeiss AG) equipped with a field-emission electron source. The overview SEM images were acquired with an acceleration voltage of 15 kV using an Everhart-Thornley detector and the high-resolution images with an acceleration voltage of 5 kV using an in-lens detector. The ZLA samples were coated with a conducting layer of ~2 nm Pt/Pd to improve the image quality on the insulating zirconia sample.

Besides material characterization, SEM imaging was applied to analyze the blood interaction with the materials surfaces. After the period of incubation in human whole blood, the samples were fixed in Karnovsky's fixing solution for 1 h at RT and washed twice in PBS. Subsequently, the samples were dehydrated by a gradient series of ethanol (30, 50, 70, 80, 90 and 100%) followed by incubation in hexamethyldisilazane (HMDS) (Sigma-Aldrich) for 30 min. After drying overnight at room temperature (RT), surfaces were gold–platinum sputtered (10 nm-thick coating, Leica EM ACE 600). Finally, SEM images were taken using a Hitachi S-4800 (Hitachi High-Technologies, Canada) at an accelerating voltage of 5 kV and 10 μA current flow. Representative images of different magnifications were taken from 2 surfaces per sample and experiment.

2.6. Serum protein adsorption

For quantification of fibrinogen adsorption and the assessment of γ-chain accessibility of adsorbed fibrinogen, per

experiement 3 samples of each titanium and zirconia surfaces were incubated in 100 μL of fibrinogen-Alexa Fluor 633 conjugate (10 μg mL^{-1} in PBS; Thermofisher) for 20 min at RT. To estimate unspecific binding of the following antibodies, reference samples were incubated for the same period of time in PBS w/o fibrinogen. After incubation surfaces were blocked by incubation with 5% goat serum and 1% FCS in PBS for 1 h. The samples were then washed in PBS and incubated in 100 μL of mouse anti-human monoclonal fibrinogen gamma antibody (1:200; IgG2a, [4H9], GeneTex). Subsequently surfaces were incubated in 100 μL of the corresponding secondary antibody, Alexa Fluor A488 conjugate (goat anti-mouse IgG2a, 1:300; ThermoFisher) for 1 h. All antibodies were dissolved in 1% FCS/PBS and stainings were performed at RT. After antibody or fibrinogen incubations surfaces were always washed 3× in PBS.

For fluorescence intensity (FI) quantification samples were analyzed employing a fluorescence microarray scanner (LS ReloadedTM, Tecan Trading AG, Switzerland) using identical settings, *i.e.* voltage, pinhole, and focal plane, for all samples per condition. FI values were determined from the obtained images *via* ImageJ, using the inner 80% surface area of the samples. Obtained FI resulting from unspecific binding of the antibodies were subtracted from measured sample FI values.

2.7. Blood incubation with partially heparinized human whole blood

Human whole blood was obtained from healthy volunteers (ethical approval BASEC Nr. PB_2016-00816 from the local ethics committee) by standard venipuncture technique. The blood was partially heparinized directly upon withdrawal into a 9 mL S-Monovette tube (neutral S-Monovette®, Sarstedt) with 3 IU mL^{-1} sodium heparin (180 IU mL^{-1}, Carl Roth) to yield a final concentration of 0.5 IU heparin mL^{-1} blood and used for the experiments within 1 h after withdrawal.

Per material 6 samples were placed into a custom device made out of polytetrafluoroethylene (PTFE, Teflon), designed as a round chamber with an inner diameter of 30 mm and 4 mm height, containing 6 cavities with an inner diameter of 5 mm and a height of 1 mm. The different sample types were always incubated in separate chambers. For the HBC cell culture studies, each chamber was filled with 2.8 mL of freshly taken human whole blood, closed with a PTFE lid, sealed with parafilm and placed on an orbital shaker (Polymax, Heidolph) at 10 rpm and 12 min (RT).

For the quantitative analysis of the blood coagulation on the surfaces, *i.e.* fibrin network formation and platelet activation, 2.8 mL of platelet-rich plasma (PRP), isolated from freshly taken human whole blood by centrifugation for 30 min at 300 g (14 °C), was filled into the PTFE chambers and samples were incubated (usually 90 min) on an orbital shaker as described above.

The incubation time was always estimated for each donor and experiment individually with a reference sample, *i.e.* SLActive, and whole blood or PRP spiked with Alexa Fluor 488-conjugated fibrinogen (final concentration 18 μg mL^{-1}) *via* epi-fluorescence microscopy (Axio Imager.M1, Carl Zeiss AG).

After the incubation, the blood was carefully removed and stabilized with Ethylenediaminetetraacetic acid (EDTA) (Sigma-Aldrich) to a final concentration of 5 mM for further analysis. Finally, the samples were rinsed gently 3× times in pre-warmed phosphate-buffered saline (PBS) (Sigma-Aldrich) before use for further experiments or analysis.

2.8. Analysis of selected molecular markers of blood coagulation

EDTA stabilized blood, taken after incubation with the material samples (6 samples of each material), was centrifuged for 10 min at 2000 × g to isolate plasma. Obtained plasma was frozen and stored at −80 °C until analysis. Commercially available enzyme-linked immunosorbent assays (ELISAs) were used to characterize blood reactions including platelet activation (platelet factor 4 (PF4), Thermofisher), coagulation activation (Prothrombin Fragment 1 + 2 (F1 + 2), USBio), and complement activation (C5a, Abcam).

2.9. Cell culture of primary human bone cells

Primary human bone cells (HBC) were isolated and cultivated as previously described [7]. In brief, femur-derived human bone marrow samples were received from healthy patients undergoing surgical hip replacement after informed consent (ethical approval was obtained ethics committee of the canton St.Gallen, CH; EKSG 08/14). Six experiments were performed with HBC of passage 2 with cells isolated from 3 different patients. Blood incubated and washed (PBS) samples were transferred into 96 well plates and 200 μL of HBC cell suspension (34,000 cells mL^{-1}) in proliferation medium (α-MEM (D-5796, Sigma-Aldrich), 10% Fetal calf serum (FCS; Lonza), 1% PSN (penicillin (5 mg mL^{-1}), streptomycin (5 mg mL^{-1}), neomycin (10 mg mL^{-1}) all from Gibco), 1 mg mL^{-1} basic fibroblast growth factor (FGF-2, F0291, Sigma-Aldrich) added to all surfaces. Cells seeded on tissue culture polystyrene (TCP) served as controls. After 24 h all samples were transferred into a new well (96 well plate) containing 200 μL of either proliferation or osteoblastic differentiation medium (α-MEM, 10% FCS, 1% PSN, 10 nM 1.25 dihydroxyvitamine D3 (D-1530, Sigma-Aldrich, freshly added when medium is changed), 50 μM ascorbic acid phosphate (A-8960, Sigma-Aldrich), 2 mM β-glycerophosphate (G-9891, Sigma-Aldrich), 10 nM dexamethasone (D-4902, Sigma-Aldrich, stock solution 1 mg mL^{-1} in 96% ethanol, freshly prepared and added when medium is changed) and incubated at 37 °C in a humidified 5% CO_2 atmosphere. Per experiment and material 3–4 surfaces were used for cell culture studies of HBCs.

2.10. Microscopy analysis of blood coagulation and HBC adhesion

For confocal laser scanning microscopy and quantification of fluorescence intensities, blood incubated samples either with or without adherent HBC were washed 3 times in PBS, fixed for 20 min in an aqueous solution of 4% PFA, 65 mM PIPES, 25 mM HEPES, 10 mM EGTA and 3 mM $MgCl_2$. To avoid unspecific binding, samples were blocked before further antibody incubation with 5% goat serum and 1% FCS in PBS for 1 h. Subsequently, activated platelets were stained *via* CD62P-selectin antibody, Alexa Fluor 645 (1:100, BioLegend)

for 1 h at RT. Next, cells were permeabilized for 10 min in PBS containing 0.1% Triton X 100. Fibrinogen was stained either by supplementation of the blood with fibrinogen-Alexa Fluor 488 conjugate (final concentration 18 $\mu g\,mL^{-1}$) during incubation of the samples or incubation with a monoclonal anti-human fibrinogen antibody (1:100, Sigma-Aldrich) for 1 h followed by incubation (1 h) with the corresponding anti-mouse Alexa Fluor 555 antibody (1:300, Thermofisher Scientific). Finally, actin and nuclei were stained with Alexa Fluor 488-conjugated phalloidin (1:40, Thermofisher) and 0.01 $mg\,mL^{-1}$ 4′,6-diamidino-2-phenylindole (DAPI, Sigma-Aldrich) for 1 h. All antibodies were dissolved in 1% FCS/PBS, stainings were performed at RT and all antibody incubation steps were followed by 3 washes with PBS.

Representative CLSM images (LSM780, Carl Zeiss AG, Switzerland) were taken at different magnifications (10× and 40×) from 2 surfaces per sample and experiment.

For quantification of fibrinogen and platelet activation (CD62P) on the surfaces, samples were analyzed with a fluorescence scanner as described above for protein adsorption.

2.11. Calcium quantification assay

HBC were cultivated on the different blood pre-incubated surfaces for a period of 28 d. In order to quantify mineralization, the HBC derived Ca^{2+} concentrations were correlated to their cell numbers as previously described by Kopf et al. [7]. In brief, the number of metabolic active HBC was determined by alamar blue (AB) assay (alamarBlue® Cell Viability Reagent; DAL1025, Invitrogen). A volume of 20 μL AB solution was added to culture medium and fluorescence intensities were measured (Mithras2 Plate reader, Berthold Technologies) after 2 h of incubation. Cell numbers were calculated by interpolating fluorescence readings from a 6-point standard curve (measured from known HBC numbers after 1 day in culture). Following the AB measurements, samples were washed twice with pre-warmed PBS and lysed in 100 μL 1 M HCl for 3 h at 37 °C under constant agitation. Afterwards, 5 μL of each lysate were transferred to a 96-well plate and 195 μL of working reagent (Quanti Chrom™ Calcium Assay DICA-500, Gentaur) were added to analyze the levels of Ca^{2+}. After 3 min, absorbance of the solution was measured at 595 nm (Biotek Instruments Elx 800, Witec AG). Samples were analyzed in triplicates and calcium concentrations were calculated by means of a standard curve.

2.12. Statistics

All data were analyzed using GraphPad Prism 6 (GraphPad Software Inc., USA) and analysis of the statistical significance between the samples was performed by two-way ANOVA (results obtained from at least three different donors) and Tukey-Kramer's post hoc test. Asterisks denote statistical significance as follows: * $p < 0.05$, ** $p < 0.01$, *** $p < 0.001$. All data are presented as mean values ± standard deviation (SD).

3. Results

3.1. Surface analyses

ZLA, SLA and SLActive samples were fabricated and the surfaces thoroughly characterized. SEM analysis showed that all surfaces exhibit microstructures with comparable dimensions of lateral features (Fig. 1). Notably however, features were shallower on zirconia as compared to titanium surfaces. Also the structures appeared different, as on titanium structures sharp and rugged peaks were obtained but on the zirconia surface more round and granular structures were formed. Randomly oriented, but homogenously distributed spontaneously formed [35] nanostructures with dimensions of about 10–30 nm were found only on SLActive surfaces, whereas on top of ZLA, granular nanostructures ranging from a few ten to several hundred nanometers could be observed.

Roughness (*i.e.* S_a and S_z) was highest for SLA and lowest for ZLA. S_{sk} measurements showed that SLA and SLActive surfaces are characterized by predominant peaks whereas ZLA is characterized by predominant depressions. (Table 1a)

Contact angle (C.A.) measurements demonstrated a hydrophobic surface for SLA and hydrophilic surfaces for ZLA and SLActive; latter surface demonstrating complete wetting with a contact angle of 0° (Table 1b).

The measurements of the surface chemistry by means of X-ray photoelectron spectroscopy (XPS) revealed the elements characteristic for the surface of the respective materials and an additional carbon contamination layer. Oxygen is observed on the titanium samples as a result of the oxidation of the surface under the formation of TiO_2. The carbon contamination (*e.g.* hydrocarbons) as well as the low level of nitrogen are a result of the exposure of the samples to air during the manufacturing process and also during sample handling for the XPS measurements. The low amounts of F on the zirconia surface are attributed to the surface treatment with HF. Overall, only expected elements from the base material and the carbon contamination layer were detected. No unexpected foreign elements were detected (Table 1c).

3.2. Surface interaction with plasma proteins

To investigate the early biological events upon implantation of materials, fibrinogen adsorption from a solution of fibrinogen in PBS buffer onto the different surfaces was evaluated and found to be lowest for SLA and highest for ZLA. On top of SLActive fibrinogen adsorption was about 2-fold higher compared to SLA but significantly lower than ZLA. However, not only the quantity of the adsorbed fibrinogen but also its conformation, which is critically affected by the surface chemistry, is important for adhesion of platelets [36]. To determine differences in the conformation of the adsorbed fibrinogen and to evaluate the possibility of platelet–fibrinogen interactions, binding of a site-specific antibody sensitive for the C-terminal region of fibrinogen γ-chain encompassing the main platelet $\alpha_{IIb}\beta_3$ integrin binding site was assessed [36,37]. As shown in Fig. 2B antibody binding was lowest for SLA and highest for ZLA. Calculating the ratio of antibody binding and total adsorbed fibrinogen (Fig. 2C), SLActive was found to support

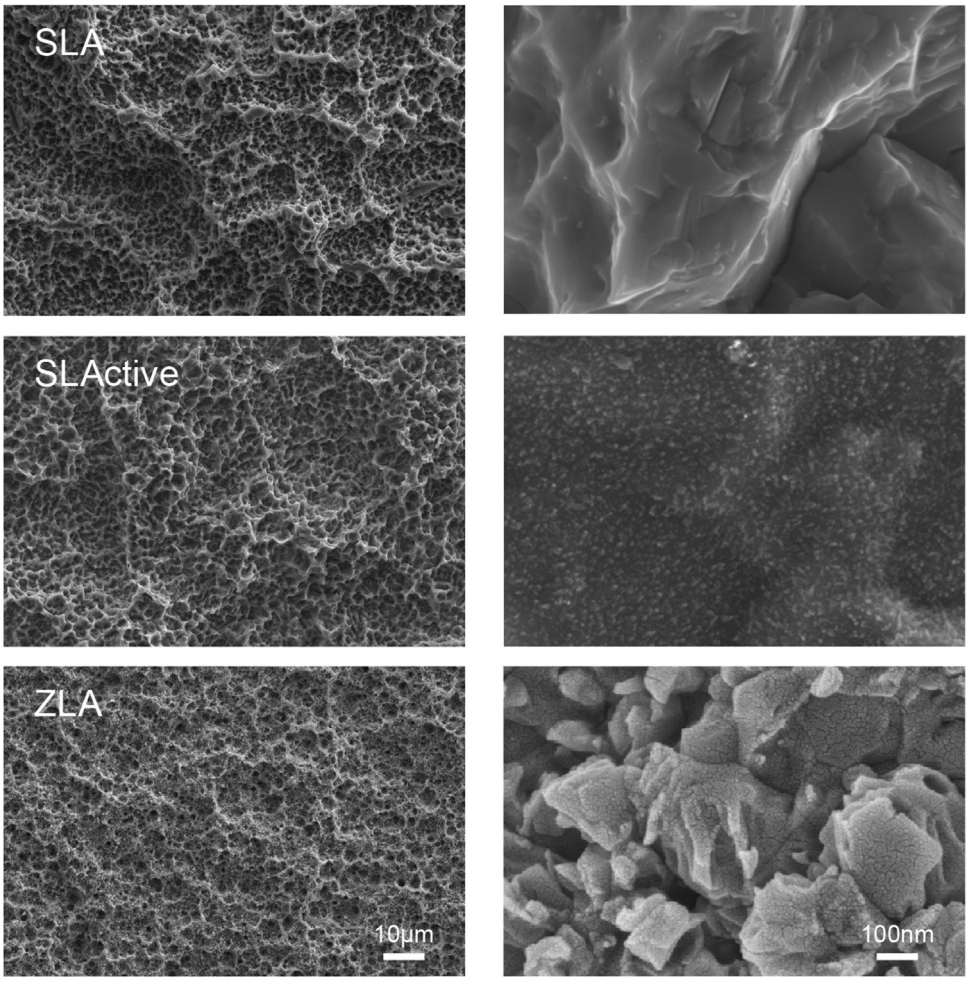

Fig. 1 – Surface characterization of the different implant materials. Scanning electron microscopy (SEM) images of SLA, SLActive, and ZLA at 2 different magnifications. Nanostructures were only present on SLActive and ZLA surfaces.

Table 1 – Physicochemical analysis of the different surfaces. All results are presented as mean (±SD) of n = 3. (a) Analysis of surface micro-roughness *via* confocal microscopy. (b) Analysis of the water contact angle on top of the different surfaces. (c) Analysis of the surface's elemental composition *via* XPS. Apparent normalized atomic concentration [%] (sum equals 100%) of the elements detected by XPS. The mean values are presented (three samples, one measurement each).

a) Surface micro-roughness

Sample	S_a [µm]	S_z [µm]	S_{sk}	S_{dr} [%]	S_{pd} [mm^{-2}]
SLA	1.46 (0.08)	20.77 (2.63)	0.16 (0.07)	16.86 (1.37)	1592 (240)
SLActive	1.29 (0.02)	18.15 (2.55)	0.11 (0.03)	13.36 (0.44)	1590 (170)
ZLA	0.71 (0.03)	9.59 (1.85)	−0.29 (0.05)	4.18 (0.35)	1798 (165)

b) Contact angle

Sample	C.A. [°]
SLA	113.6 (25.6)
SLActive	0 (0)
ZLA	6.4 (0.4)

c) Elemental composition

Sample	C [%]	F [%]	N [%]	O [%]	Ti [%]	Y [%]	Zr [%]
SLA	45.7 (2.8)	–	2.9 (0.3)	38.2 (2.0)	13.2 (1.1)	–	–
SLActive	10.6 (0.2)	–	1.5 (0.1)	62.2 (0.1)	25.7 (0.2)	–	–
ZLA	24.5 (2.3)	1.1 (0.2)	–	47.3 (2.3)	–	1.2 (0.1)	25.9 (0.7)

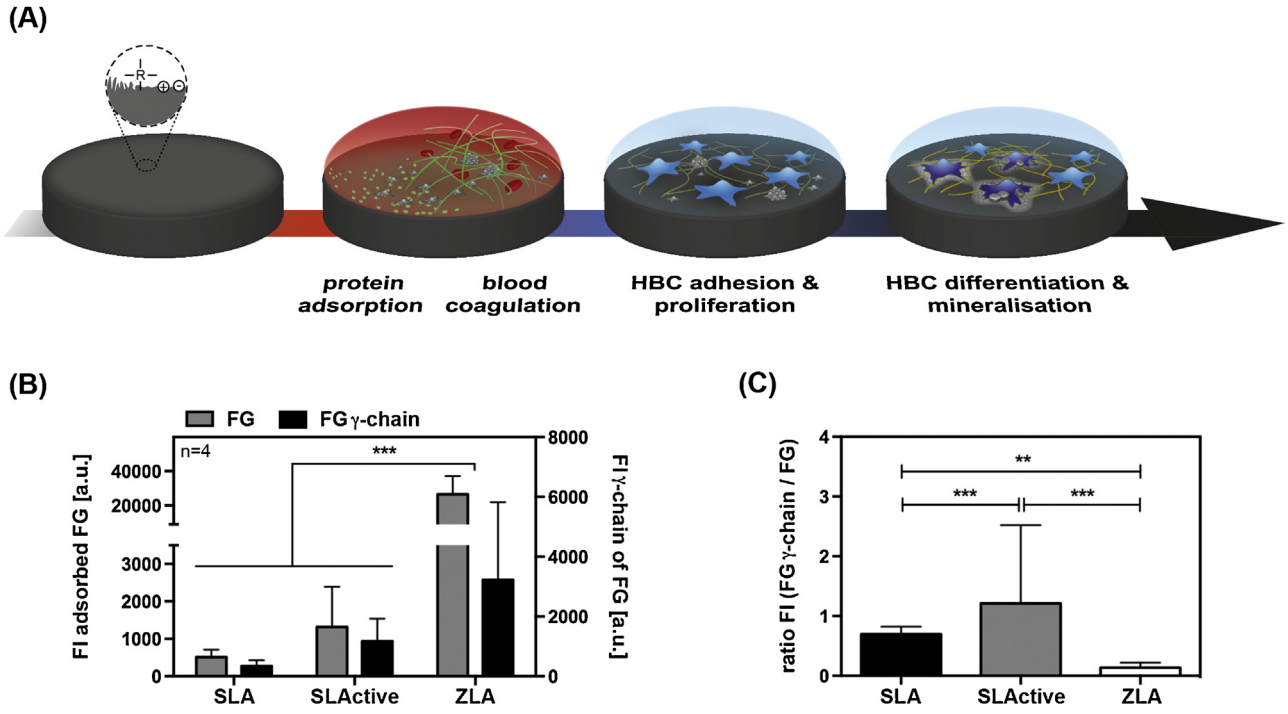

Fig. 2 – (A) Schematic illustration of the advanced in vitro model including a blood incubation step prior HBC culture on top of the material's surface. (B) Fibrinogen (FG) adsorption as a function of the dental implant material and surface modification. Fibrinogen adsorption and antibody-accessibility of the fibrinogen C-terminal region of the γ-chain were analyzed *via* immunohistochemistry and obtained fluorescence intensities (FI) measured with a microarray scanner. (C) Based on measured FI values, the ratio of γ-chain antibody staining and fibrinogen was calculated. Data are presented as mean ± SD of n = 4. Asterisks denote statistical significance: ** $p < 0.01$ and *** $p < 0.001$.

the protein conformation that allows antibody-accessibility of the γ-chain best. Even though highest fibrinogen concentrations were observed on top of ZLA, the percentage of molecules with accessible γ-chain was lowest.

3.3. *Surface interaction with whole blood*

To analyze the impact of material and surface modifications on blood coagulation, titanium and zirconia surfaces were incubated in human whole blood and evaluated for thrombus formation (Fig. 3A). On top of hydrophobic SLA surfaces, platelet adhesion and partial aggregation were visible, but largely without formation of fibrin. On the contrary pronounced blood coagulation, as seen by significant levels of fibrin network and platelet aggregates, was obtained on top of the hydrophilic SLActive and ZLA surfaces. In particular, on top of the zirconia surface a dense layer of fibrin was obtained whereas on top of the SLActive surface a more loosely arranged thrombus was observed. Analysis of the fibrin concentrations on top of the different surfaces after incubation in platelet-rich plasma (PRP) *via* immunohistochemistry and a microarray scanner could confirm the trend seen in the SEM images (Fig. 3B,C). Lowest fluorescence intensities (FI) were measured for SLA and highest for ZLA. In addition, platelet activation as a function of the material was analyzed by measuring the levels of CD62P, a prominent marker for platelet activation, *via* antibody staining. As shown in Fig. 3C lowest FI were measured for SLA and highest for ZLA.

In addition to microscopy and immunohistochemical analysis of the surfaces, selected molecular markers of the coagulation cascade were analyzed in the supernatants after incubation of the surfaces in whole blood *via* ELISA. Platelet activation, determined by released levels of platelet factor 4 (PF4), was highest for ZLA and lowest for SLA. Results for coagulation activation, determined by concentration of prothrombin fragments 1 + 2 (F1/F2), were comparable to those for PF4. Contrasting the results obtained from fibrin quantification, only slight differences between the two titanium surfaces were obtained for the thrombin activation F1/F2. Analysis of the complement cascade activation, *i.e.* C5a, showed no measurable differences between the different surfaces.

3.4. *Adhesion and osteogenic differentiation of HBC cultured on surfaces pre-incubated with human whole blood*

To assess the initial cell attachment of primary human HBC on whole blood incubated surfaces, the samples were analyzed *via* confocal laser scanning microscopy (CLSM) after 24 h (Fig. 4A). Homogenous cell attachment, well spread cytoskeleton, and exhibition of long filopodia were observed on all samples. After 28 d of culture the number of metabolically active cells and produced Ca^{2+} per surface levels were determined. Mineralization of the HBC was assessed by determining the ratio of measured calcium levels and cell numbers. As seen in Fig. 4B (top) highest levels of calcium were obtained

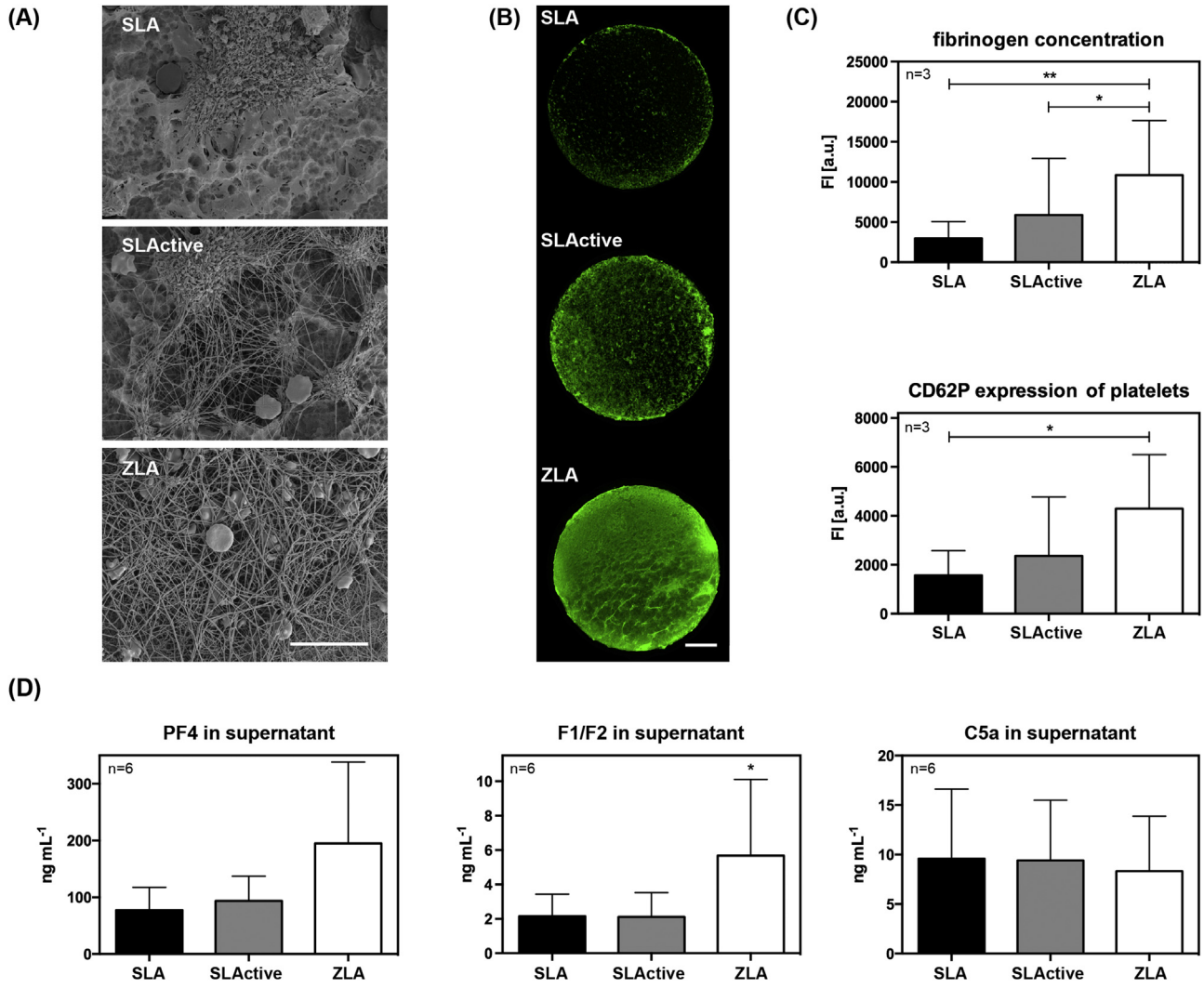

Fig. 3 – Blood coagulation on the implant surface samples after incubation in partially heparinized whole blood or PRP. Fibrin network formation on the different implant surfaces after whole blood incubation was evaluated by (A) SEM imaging (scale bar 20 μm) and after incubation in PRP by (B) a microarray scanner (scale bar 1 mm) after staining of fibrinogen (green). (C) Fibrin and platelet activation (CD62P) were quantified with a microarray scanner. (D) Selected molecular markers of the coagulation cascade, *i.e.* PF4, F1/F2, and C5a, were analyzed in the supernatants of the whole blood incubated surfaces *via* ELISA. Data are presented as mean ± SD. Asterisks denote statistical significance: * $p < 0.05$, ** $p < 0.01$. (For interpretation of the references to colour in this figure legend, the reader is referred to the web version of this article.).

with HBC on top of SLActive surfaces and lowest on top of SLA. Notably calcium levels on top of ZLA were higher compared to SLA but lower in comparison to SLActive. Estimation of metabolically active cells at day 28 showed only slight differences between the surfaces being 1.2–1.4 fold higher on zirconia compared to the titanium surfaces. Analysis of calcium levels per 1000 cells revealed the same trend (Fig. 4B).

4. Discussion

The aim of this work was to study how the interaction of a microstructured zirconia surface with blood influences its osseointegration potential when compared to state of the art titanium surfaces with similar surface topographies. For that purpose, a set of well-defined surfaces was fabricated and an advanced *in vitro* model for osseointegration that encompasses a blood incubation step prior to cell seeding and cultivation was applied.

Zirconia surface characteristics were assessed using SEM, XPS, contact angle studies and surface roughness measurements. According to the definition by Wennerberg and Albrektsson, both titanium surfaces are moderately rough (Sa 1–2 μm) whereas the zirconia surface is minimally rough (Sa 0.5–1 μm) [21]. Wennerberg and Albrektsson observed that moderately rough surfaces are preferred for titanium based dental implants, as this leads to higher osseointegration potential compared to implants with lower or higher roughness [21]. Furthermore, the material properties and fabrication techniques led to surface microstructures being characterized

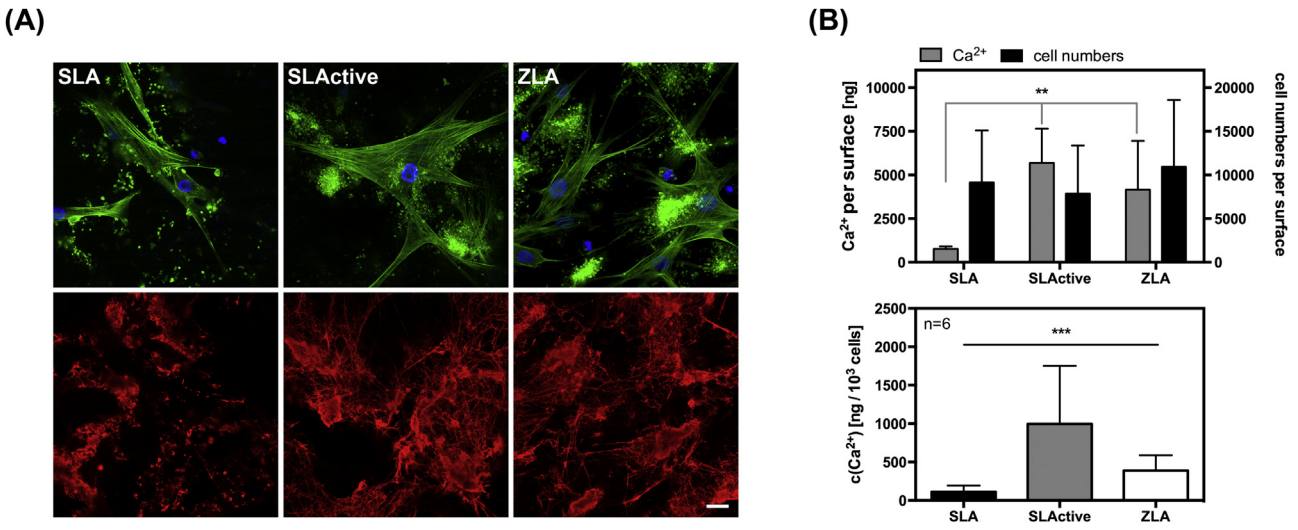

Fig. 4 – HBC cultured on top of implant surfaces pre-incubated in whole blood and the osseointegration potential of the surfaces analyzed. (A) Cell adhesion after 24 h of culture was investigated with confocal microscopy after staining of the fibrin network (red), the actin cytoskeleton (green) and nuclei (blue) (scale bar 20 μm). (B) After a culture period of 28d numbers of metabolically active cells were measured, the calcium levels were quantified (both top) and calcium levels per 1000 cells were calculated (bottom). Data are presented as mean ± SD of n = 6. Asterisks denote statistical significance as follows: ** $p < 0.01$ and *** $p < 0.001$. (For interpretation of the references to colour in this figure legend, the reader is referred to the web version of this article.).

by sharp and rugged peaks on titanium but more round, granular shaped microstructures on ZLA. In agreement to previous reports, no nanostructures were observed on SLA, and randomly oriented "spike" shaped nanostructures on SLActive that are homogenously distributed [35]. These nanostructures are composed of titanium dioxide and are a result of the storage in aqueous solution [35]. In contrast, polydisperse and granular shaped nanostructures were found on top of ZLA because of the acid attack exposing individual grains of the base material on the surface. SLA surfaces were hydrophobic and SLActive surfaces displayed a hydrophilic character, matching previous reports [6,33]. While the zirconia surface used within this study had hydrophilic properties similar to previously reported oxygen plasma treated zirconia surfaces, these surfaces shift toward hydrophobic within a period of several months due to contamination by carbon species as summarized in Caravaca et al. [28]. This change of wettability was prevented within this study using freshly prepared and H_2O_2-plasma sterilized surfaces.

In vivo, the adsorption of plasma proteins from blood on the implant surface is the first event to occur and it is through this layer that blood coagulation is initiated and cells respond toward the biomaterial. In this study, adsorption of fibrinogen, a predominant plasma protein, was evaluated. However, not only adsorption but more importantly the conformation of fibrinogen is key in the biomaterial induced thrombosis, as this determines binding of platelet integrin receptors leading to adhesion, activation, and aggregation of the platelets [36–38]. Furthermore, being the precursor to fibrin, fibrinogen is the central building block of the blood clot. Surface hydrophilicity and material chemistry were found to have a strong impact on the interactions between fibrinogen and the different dental implants. Fibrinogen adsorption was increased on hydrophilic surfaces, which is in agreement with a previous report [33] and was drastically increased on the zirconia surface in comparison to both titanium surfaces. Recently, Rezwan et al. reported that on top of titanium nanoparticle surfaces electrostatic forces dominate the protein adsorption of lysozyme and BSA from an aqueous suspension, whereas on zirconia nanoparticle surfaces also hydrophobic interactions are added to the surface's electrostatic forces, leading to increased amounts of protein adsorption [39]. While this observation might also explain the increased protein adsorption on the here presented zirconia surface, it is well accepted that the conformation of fibrinogen, which is critically affected by the surface chemistry, too, is more important for adhesion of the platelets than the total amount of surface adsorbed protein [36]. Especially the 12-amino acid sequence encompassing residues 400–411 of the C-terminal region of the fibrinogen γ-chain has been identified to interact with platelet $\alpha_{IIb}\beta_3$ integrin [37,40,41]. Furthermore, the C-terminal region of the γ-chain is sufficient for fibrin stabilization as Factor XIIIa enzymatically crosslinks opposing C-terminal segments of the γ-chain [40]. Therefore, the biological accessibility of the fibrinogen γ-chain was analyzed *via* specific antibody staining. The material's influence on the fibrinogen conformation was similar to the trend of measured total fibrinogen with higher levels of antibody-accessible fibrinogen γ-chain on ZLA compared to SLActive, and SLA respectively, which had lowest measurable levels. High levels of exposed fibrinogen γ-chain on top of the zirconia samples could be either the result of the high levels of adsorbed proteins or due to increased hydrophobic interactions between surface and protein. Recently, studies applying self-assembled monolayer (SAM) surfaces could demonstrate that fibrinogen adsorption to hydrophobic surfaces resulted in highest conformational

changes, *i.e.* loss of α-helix, of the proteins along with greatest numbers of adherent platelets [36]. Determining the relative concentration of the γ-chain revealed highest levels for SLActive and lowest for ZLA. Low relative levels of exposed γ-chain on top of the zirconia surface may be the result of the high levels of protein that either prevent the access of the antibody to the γ-chain due to fibrinogen multilayers, also known to reduce cell adhesion [38], or due to the dense packing of fibrinogen that could influence conformational changes of the proteins toward less exposed levels of fibrinogen γ-chain. Contrasting this, adsorption of fibrinogen at low density, was shown to promote platelet adhesion [38], which is reflected in the current study by highest relative levels of γ-chain domains on SLActive. Since blood coagulation and thrombus formation on biomaterial surfaces is triggered immediately after coverage with a layer of plasma proteins, it appears that the high levels of total accessible fibrinogen γ-chain for ZLA surfaces yield increased platelet adhesion and activation, thus causing higher thrombogenicity of zirconia compared to titanium surfaces. This was further investigated with *in vitro* whole blood incubation studies.

During the chosen incubation time, only rare spots of platelet aggregates and fibrin were obtained on top of SLA, while a dense network of fibrin was detected on SLActive. Notably, the thickest thrombus layer was observed on top of ZLA. This was also reflected in levels of platelet activation (CD62P, PF4) and activation of thrombin (F1/F2). Increased coagulation and fibrin deposition on top of sandblasted, acid etched titanium has been previously reported for superhydrophilic surfaces, if compared to hydrophobic titanium surfaces [7,33,34,42,43]. Interestingly, thrombus formation is even more pronounced on the hydrophilic zirconia surface (Fig. 3A). Similar observations of enhanced blood coagulation on a titanium-zirconium alloy in comparison to titanium was reported previously [33]. Taking into account that the total accessibility of adsorbed fibrinogen was highest for ZLA, and so were the levels of platelet activation, it appears that the increased levels of blood coagulation on top of the zirconia sample are the result of increased platelet adhesion, which leads to their activation and thus triggers the coagulation cascade. This is supported by more fibrin being present and higher concentrations of CD62P and PF4 along with higher levels of total accessible fibrinogen γ-chain that were observed on SLActive compared to SLA.

Besides protein conformation, the pure physicochemical properties of the different materials could also account to the strong activation of coagulation on zirconia, *e.g. via* contact activation. Several studies have demonstrated that platelet adhesion and activation of coagulation on biomaterials is governed by synergistic levels of hydrophobic and hydrophilic functional moieties on the surface [44,45]. As reported above, in addition to electrostatic forces, hydrophobic ones are also important for the protein interactions at zirconia surfaces. Therefore, the results suggest that the level of the interplay of hydrophobic and hydrophilic forces on ZLA activates coagulation more compared to SLActive, *i.e. via* increased activation of the intrinsic pathway of coagulation [46]. Complement activation (C5a) was similar for all surfaces within the analyzed time period and has thus not been further studied in this work.

Obtained blood clots on top of the surfaces provide the first provisional extracellular matrix (ECM) and the spatiotemporal organization of soluble, *e.g.* platelet derived cytokines, and adhesive cues affects the subsequent steps of wound healing and implant integration [32]. Analyzing the osseointegration potential of the different surfaces, homogenous HBC attachment was obtained on all whole blood pre-incubated surfaces after 24 h of culture. Besides the platelet binding sequence in the γ-chain, human fibrinogen contains two further putative β_3 integrin binding sites within the α-chain, *i.e.* RGDF (Aα95-97) and RGDS (Aα572-574)[37,47]. Due to the incubation in whole blood, at least plasma fibrinogen, in case no fibrin was formed, adsorbed to all surfaces, which can explain why HBC attachment was obtained on all surfaces. In addition, other adhesive ECM proteins such as vitronectin or fibronectin are likely to be found on the surface and within the provisional ECM and could increase cell attachment. Notably, analysis with CLSM showed highest numbers of adherent cells on the zirconia surface (data not shown). This correlates to the observation that the fibrin network appeared most dense on ZLA surfaces, which provides a high local density of adhesion motifs that allow cellular attachment and spreading.

However, even though ZLA surfaces were homogenously covered by fibrin and adherent HBC, the observed calcium level after 28 d of culture was lower compared to SLActive, but still increased when compared to SLA. The differences obtained between the two titanium surfaces are in agreement to previous *in vitro* and *in vivo* observations and reported mechanisms involved in the response of HBC toward the materials surface include for instance Wnt signaling pathway and integrin signaling [6,7,48,49]. The observed difference between HBC differentiation on zirconia and titanium surfaces have not been reported so far and are probably due to variations in surface topography and surface physicochemical properties. In several reports, it was demonstrated how variations in micro- and nanostructure and their degree of order affect the osteogenic differentiation of HBC [50–52]. Thereby, $\alpha_2\beta_1$ integrin expression and signaling has been identified as an important mechanism driving cell fate decisions of the HBC [49]. As seen in the SEM images, (Fig. 1) the micro- and nanostructures of the zirconia surface have a different size and morphology in comparison to the titanium surfaces. In addition, the different implant surface chemistries and topographies were shown to influence protein adsorption and conformation of fibrinogen on top of the surfaces within this study. A similar surface influence on protein quantity and folding could also be expected for other key proteins of the ECM, *e.g.* fibronectin, whose secondary structure was also demonstrated to depend on the surface properties [53]. As the HBC respond toward the materials by sensing the adsorbed protein layer at the microstructured surfaces, it can be expected that the altered interactions between proteins and the surface in combination with the different topography in case of the zirconia surface result in a different cell fate decision *via* altered integrin clustering compared to surfaces of titanium [54]. Thrombus formation on the surfaces also has an important influence on HBC fate decisions [7], providing not only adhesion ligands but also a plethora of soluble cues which are released during platelet activation and temporarily associated to the fibrin network [55]. Several of the platelet derived

cytokines, *e.g.* isoforms of TGF-β or PDGF, are involved in HBC migration and differentiation [56–58] and are released over the course of tissue regeneration and matrix remodeling [59]. The detailed composition of the blood clot is unique for each material and determined by the dynamics of coagulation depending on the interactions of material surface and blood. However, the fibrin matrix is only temporary and is degraded within a few days by the cells and replaced by their own ECM. Thereby, the bound fraction of cytokines is released into the culture medium resulting in a rather short-lived stimulus serving only as an initial trigger of HBC fate decisions. In view of the material dependent fibrin — cytokine composition, it could be considered that the cytokine cocktail bound to the fibrin matrix on the ZLA surface has a less well balanced composition to stimulate the early HBC differentiation when compared to the SLActive surface. However, the detailed composition of the obtained fibrin matrices and/or adsorbed cytokines has to be investigated in more detail to answer this question.

5. Conclusions

In this study, a microstructured zirconia surface was fabricated and compared to well established titanium implants. While fibrinogen adsorption was significantly increased on the zirconia surface, along with the highest thrombogenicity in comparison to both titanium surfaces, the osseointegration potential of ZLA after 28 d was lower compared to SLActive but was significantly increased in comparison to SLA. The results suggest that the influence of the ZLA surface chemistry on protein folding in combination with the topographical features is responsible for the lower osteogenic differentiation of the HBC, most likely *via* altered integrin signaling. Furthermore, it appears that surfaces with increased thrombogenicity offer an enhanced osseointegration potential. The total quantity of obtained thrombus is however not 1:1 correlated to HBC mineralization and warrants a detailed investigation into the biomolecular composition of the thrombus and underlying mechanisms how the molecular cues balance HBC fate decisions. However, previously reported *in vivo* data [6,22,60,61] are in agreement with the herein demonstrated *in vitro* results. Therefore, the employed *in vitro* approach is highly relevant for implant development, as it allows to predict the *in vivo* osseointegration potential of different bulk materials and surface modifications.

Disclosures

The authors declare no conflict of interest. Simon Berner and Marc Stephan are currently employees of Straumann and participated in the study as contributing scientists. The study was funded by CTI (Grant No: 16873.2 PFNM-NM). Institut Straumann AG (Basel, Switzerland) solely provided sample discs for the study and had no role in study design.

Acknowledgments

We thank the Swiss Commission for Technology and Innovation CTI (Grant No: 16873.2 PFNM-NM) for financial support. We also like to thank Ursina Tobler for her valuable support in the laboratory work during the study.

REFERENCES

[1] Ananth H, Kundapur V, Mohammed HS, Anand M, Amarnath GS, Mankar S. A review on biomaterials in dental implantology. Int J Biomed Sci 2015;11:113–20.
[2] Smeets R, Stadlinger B, Schwarz F, Beck-Broichsitter B, Jung O, Precht C, et al. Impact of dental implant surface modifications on osseointegration. BioMed Res Int 2016;2016:16.
[3] Lohmann CH, Bonewald LF, Sisk MA, Sylvia VL, Cochran DL, Dean DD, et al. Maturation state determines the response of osteogenic cells to surface roughness and 1,25-dihydroxyvitamin D3. J Bone Miner Res 2000;15:1169–80.
[4] Martin JY, Dean DD, Cochran DL, Simpson J, Boyan BD, Schwartz Z. Proliferation, differentiation, and protein synthesis of human osteoblast-like cells (MG63) cultured on previously used titanium surfaces. Clin Oral Implants Res 1996;7:27–37.
[5] Li D, Ferguson SJ, Beutler T, Cochran DL, Sittig C, Hirt HP, et al. Biomechanical comparison of the sandblasted and acid-etched and the machined and acid-etched titanium surface for dental implants. J Biomed Mater Res 2002;60:325–32.
[6] Wennerberg A, Jimbo R, Stübinger S, Obrecht M, Dard M, Berner S. Nanostructures and hydrophilicity influence osseointegration: a biomechanical study in the rabbit tibia. Clin Oral Implants Res 2014;25:1041–50.
[7] Kopf BS, Schipanski A, Rottmar M, Berner S, Maniura-Weber K. Enhanced differentiation of human osteoblasts on Ti surfaces pre-treated with human whole blood. Acta Biomater 2015;19:180–90.
[8] Wennerberg A, Galli S, Albrektsson T. Current knowledge about the hydrophilic and nanostructured SLActive surface. Clin Cosmet Investig Dent 2011;3:59–67.
[9] Oates TW, Valderrama P, Bischof M, Nedir R, Jones A, Simpson J, et al. Enhanced implant stability with a chemically modified SLA surface: a randomized pilot study. Int J Oral Maxillofac Implants 2007;22:755–60.
[10] van Velzen FJJ, Ofec R, Schulten EAJM, ten Bruggenkate CM. 10-year survival rate and the incidence of peri-implant disease of 374 titanium dental implants with a SLA surface: a prospective cohort study in 177 fully and partially edentulous patients. Clin Oral Implants Res 2015;26:1121–8.
[11] Lang NP, Salvi GE, Huynh-Ba G, Ivanovski S, Donos N, Bosshardt DD. Early osseointegration to hydrophilic and hydrophobic implant surfaces in humans. Clin Oral Implants Res 2011;22:349–56.
[12] Greenbaum DS, Masri R, Driscoll CF. Prosthodontic rehabilitation of dental implants with exposed threads: a clinical report. J Prosthet Dent 2011;105:351–5.
[13] Thoma DS, Buranawat B, Hämmerle CH, Held U, Jung RE. Efficacy of soft tissue augmentation around dental implants and in partially edentulous areas: a systematic review. J Clin Periodontol 2014;41(Suppl 15):S77–91.
[14] Sanz-Martin I, Sailer I, Hämmerle CH, Thoma DS. Soft tissue stability and volumetric changes after 5 years in pontic sites with or without soft tissue grafting: a retrospective cohort study. Clin Oral Implants Res 2016;27:969–74.
[15] Schneider D, Grunder U, Ender A, Hämmerle CH, Jung RE. Volume gain and stability of peri-implant tissue following bone and soft tissue augmentation: 1-year results from a

prospective cohort study. Clin Oral Implants Res 2011;22:28–37.
[16] Javed F, Al-Hezaimi K, Almas K, Romanos GE. Is titanium sensitivity associated with allergic reactions in patients with dental implants? A systematic review. Clin Implant Dent Relat Res 2013;15:47–52.
[17] Sicilia A, Cuesta S, Coma G, Arregui I, Guisasola C, Ruiz E, et al. Titanium allergy in dental implant patients: a clinical study on 1500 consecutive patients. Clin Oral Implants Res 2008;19:823–35.
[18] Piconi C, Maccauro G. Zirconia as a ceramic biomaterial. Biomaterials 1999;20:1–25.
[19] Cionca N, Hashim D, Mombelli A. Zirconia dental implants: where are we now, and where are we heading? Periodontol 2000 2017;73:241–58.
[20] Gahlert M, Gudehus T, Eichhorn S, Steinhauser E, Kniha H, Erhardt W. Biomechanical and histomorphometric comparison between zirconia implants with varying surface textures and a titanium implant in the maxilla of miniature pigs. Clin Oral Implants Res 2007;18:662–8.
[21] Wennerberg A, Albrektsson T. Effects of titanium surface topography on bone integration: a systematic review. Clin Oral Implants Res 2009;20:172–84.
[22] Gahlert M, Roehling S, Sprecher CM, Kniha H, Milz S, Bormann K. In vivo performance of zirconia and titanium implants: a histomorphometric study in mini pig maxillae. Clin Oral Implants Res 2012;23:281–6.
[23] Gahlert M, Röhling S, Wieland M, Eichhorn S, Küchenhoff H, Kniha H. A comparison study of the osseointegration of zirconia and titanium dental implants. A biomechanical evaluation in the maxilla of pigs. Clin Implant Dent Rela Res 2010;12:297–305.
[24] Linares A, Grize L, Munoz F, Pippenger BE, Dard M, Domken O, et al. Histological assessment of hard and soft tissues surrounding a novel ceramic implant: a pilot study in the minipig. J Clin Periodontol 2016;43:538–46.
[25] Pieralli S, Kohal RJ, Lopez Hernandez E, Doerken S, Spies BC. Osseointegration of zirconia dental implants in animal investigations: a systematic review and meta-analysis. Dent Mater 2018;34:171–82.
[26] Bergemann C, Duske K, Nebe JB, Schöne A, Bulnheim U, Seitz H, et al. Microstructured zirconia surfaces modulate osteogenic marker genes in human primary osteoblasts. J Mater Sci Mater Med 2015;26:26.
[27] Att W, Takeuchi M, Suzuki T, Kubo K, Anpo M, Ogawa T. Enhanced osteoblast function on ultraviolet light-treated zirconia. Biomaterials 2009;30:1273–80.
[28] Caravaca C, Shi L, Balvay S, Rivory P, Laurenceau E, Chevolot Y, et al. Direct silanization of zirconia for increased biointegration. Acta Biomater 2016;46:323–35.
[29] Turbill P, Beugeling T, Poot AA. Proteins involved in the Vroman effect during exposure of human blood plasma to glass and polyethylene. Biomaterials 1996;17:1279–87.
[30] Markiewski MM, Nilsson B, Nilsson Ekdahl K, Mollnes TE, Lambris JD. Complement and coagulation: strangers or partners in crime? Trends Immunol 2007;28:184–92.
[31] Gorbet MB, Sefton MV. Biomaterial-associated thrombosis: roles of coagulation factors, complement, platelets and leukocytes. Biomaterials 2004;25:5681–703.
[32] Laurens N, Koolwijk P, De Maat MPM. Fibrin structure and wound healing. J Thromb Haemost 2006;4:932–9.
[33] Kopf BS, Ruch S, Berner S, Spencer ND, Maniura-Weber K. The role of nanostructures and hydrophilicity in osseointegration: in-vitro protein-adsorption and blood-interaction studies. J Biomed Mater Res A 2015;103:2661–72.
[34] Milleret V, Tugulu S, Schlottig F, Hall H. Alkali treatment of microrough titanium surfaces affects macrophage/monocyte adhesion, platelet activation and architecture of blood clot formation. Eur Cells Mater 2011;21:430–44, discussion 44.
[35] Wennerberg A, Svanborg LM, Berner S, Andersson M. Spontaneously formed nanostructures on titanium surfaces. Clin Oral Implants Res 2013;24:203–9.
[36] Sivaraman B, Latour RA. The relationship between platelet adhesion on surfaces and the structure versus the amount of adsorbed fibrinogen. Biomaterials 2010;31:832–9.
[37] Farrell DH, Thiagarajan P, Chung DW, Davie EW. Role of fibrinogen alpha and gamma chain sites in platelet aggregation. Proc Natl Acad Sci U S A 1992;89:10729–32.
[38] Safiullin R, Christenson W, Owaynat H, Yermolenko IS, Kadirov MK, Ros R, et al. Fibrinogen matrix deposited on the surface of biomaterials acts as a natural anti-adhesive coating. Biomaterials 2015;67:151–9.
[39] Rezwan K, Studart AR, Vörös J, Gauckler LJ. Change of ζ potential of biocompatible colloidal oxide particles upon adsorption of bovine serum albumin and lysozyme. J Phys Chem B 2005;109:14469–74.
[40] Ware S, Anderson WF, Donahue JP, Hawiger J. Structure of the fibrinogen γ-chain integrin binding and factor XIIIa cross-linking sites obtained through carrier protein driven crystallization. Protein Sci 1999;8:2663–71.
[41] Springer TA, Zhu J, Xiao T. Structural basis for distinctive recognition of fibrinogen γC peptide by the platelet integrin α(IIb)β(3). J Cell Biol 2008;182:791–800.
[42] Hong J, Kurt S, Thor A. A hydrophilic dental implant surface exhibit thrombogenic properties in vitro. Clin Implant Dent Relat Res 2013;15:105–12.
[43] Burkhardt MA, Waser J, Milleret V, Gerber I, Emmert MY, Foolen J, et al. Synergistic interactions of blood-borne immune cells, fibroblasts and extracellular matrix drive repair in an in vitro peri-implant wound healing model. Sci Rep 2016;6:21071.
[44] Rodrigues SN, Gonçalves IC, Martins MCL, Barbosa MA, Ratner BD. Fibrinogen adsorption, platelet adhesion and activation on mixed hydroxyl-/methyl-terminated self-assembled monolayers. Biomaterials 2006;27:5357–67.
[45] Sperling C, Fischer M, Maitz MF, Werner C. Blood coagulation on biomaterials requires the combination of distinct activation processes. Biomaterials 2009;30:4447–56.
[46] Tengvall P, Askendal A. Ellipsometric in vitro studies on blood plasma and serum adsorption to zirconium. J Biomed Mater Res 2001;57:285–90.
[47] Doolittle RF, Watt KW, Cottrell BA, Strong DD, Riley M. The amino acid sequence of the alpha-chain of human fibrinogen. Nature 1979;280:464–8.
[48] Olivares-Navarrete R, Hyzy SL, Park JH, Dunn GR, Haithcock DA, Wasilewski CE, et al. Mediation of osteogenic differentiation of human mesenchymal stem cells on titanium surfaces by a Wnt-integrin feedback loop. Biomaterials 2011;32:6399–411.
[49] Olivares-Navarrete R, Raz P, Zhao G, Chen J, Wieland M, Cochran DL, et al. Integrin alpha2beta1 plays a critical role in osteoblast response to micron-scale surface structure and surface energy of titanium substrates. Proc Natl Acad Sci U S A 2008;105:15767–72.
[50] Dalby MJ, McCloy D, Robertson M, Wilkinson CD, Oreffo RO. Osteoprogenitor response to defined topographies with nanoscale depths. Biomaterials 2006;27:1306–15.
[51] Zhukova Y, Hiepen C, Knaus P, Osterland M, Prohaska S, Dunlop JWC, et al. The role of titanium surface nanostructuring on preosteoblast morphology, adhesion, and migration. Adv Healthcare Mater 2017;6:2192–659.
[52] Dalby MJ, Gadegaard N, Tare R, Andar A, Riehle MO, Herzyk P, et al. The control of human mesenchymal cell

differentiation using nanoscale symmetry and disorder. Nat Mater 2007;6:997–1003.
[53] Afara N, Omanovic S, Asghari-Khiavi M. Functionalization of a gold surface with fibronectin (FN) covalently bound to mixed alkanethiol self-assembled monolayers (SAMs): the influence of SAM composition on its physicochemical properties and FN surface secondary structure. Thin Solid Films 2012;522:381–9.
[54] Huang J, Grater SV, Corbellini F, Rinck S, Bock E, Kemkemer R, et al. Impact of order and disorder in RGD nanopatterns on cell adhesion. Nano Lett 2009;9:1111–6.
[55] Amable PR, Carias RBV, Teixeira MVT, da Cruz Pacheco Í, Corrêa do Amaral RJF, Granjeiro JM, et al. Platelet-rich plasma preparation for regenerative medicine: optimization and quantification of cytokines and growth factors. Stem Cell Res Ther 2013;4:67.
[56] Fiedler J, Roderer G, Gunther KP, Brenner RE. BMP-2, BMP-4, and PDGF-bb stimulate chemotactic migration of primary human mesenchymal progenitor cells. J Cell Biochem 2002;87:305–12.
[57] Tang Y, Wu X, Lei W, Pang L, Wan C, Shi Z, et al. TGF-[beta]1-induced migration of bone mesenchymal stem cells couples bone resorption with formation. Nat Med 2009;15:757–65.
[58] Chen G, Deng C, Li YP. TGF-beta and BMP signaling in osteoblast differentiation and bone formation. Int J Bio Sci 2012;8:272–88.
[59] Sánchez-Ilárduya MB, Trouche E, Tejero R, Orive G, Reviakine I, Anitua E. Time-dependent release of growth factors from implant surfaces treated with plasma rich in growth factors. J Biomed Mater Res A 2013;101A:1478–88.
[60] Depprich R, Zipprich H, Ommerborn M, Naujoks C, Wiesmann HP, Kiattavorncharoen S, et al. Osseointegration of zirconia implants compared with titanium: an in vivo study. Head Face Med 2008;4:30.
[61] Bormann K-H, Gellrich N-C, Kniha H, Dard M, Wieland M, Gahlert M. Biomechanical evaluation of a microstructured zirconia implant by a removal torque comparison with a standard Ti-SLA implant. Clin Oral Implants Res 2012;23:1210–6.